HHS Public Access

Author manuscript

Nucl Med Biol. Author manuscript; available in PMC 2019 July 01.

Published in final edited form as:

Nucl Med Biol. 2018 ; 62-63: 1–8. doi:10.1016/j.nucmedbio.2018.05.003.

The impact of age on radium-223 distribution and an evaluation of molecular imaging surrogates

Wen Jiang[1], **David Ulmert**[2], **Brian W. Simons**[3,4], **Diane S. Abou**[5,*], and **Daniel LJ Thorek**[5,6,*]

[1]Department of Biomedical Engineering, Johns Hopkins University

[2]Department of Radiology, Memorial Sloan Kettering Cancer Center

[3]Department of Molecular and Comparative Pathobiology, Johns Hopkins University

[4]Department of Urology, Johns Hopkins University School of Medicine

[5]Division of Nuclear Medicine and Molecular Imaging, Department of Radiology, Johns Hopkins University School of Medicine

[6]Department of Oncology, Sidney Kimmel Comprehensive Cancer Center, Johns Hopkins University School of Medicine

Abstract

Introduction—Radium-223 dichloride is the first alpha-particle emitting therapeutic agent approved by FDA and EMA for bone metastatic castration-resistant prostate cancer. We studied its age-dependent biodistribution in mice, and compared it with [^{99m}Tc]Tc-MDP and [^{18}F]NaF aiming to identify a potential imaging surrogate to predict [^{223}Ra]$RaCl_2$ whole-body localization.

Methods—Male C57Bl/6 mice dosed with [^{223}Ra]$RaCl_2$ were sacrificed at different time points to explore [^{223}Ra]$RaCl_2$ whole-body distribution. In another experiment, mice at different ages were dosed with [^{223}Ra]$RaCl_2$ to evaluate the aging impact. Finally, [^{99m}Tc]Tc-MDP and [^{18}F]NaF were administered to mice, and we compared their biodistributions with [^{223}Ra]$RaCl_2$. Detailed micro-localization of each tracer was visualized using autoradiography and histochemical staining.

Results—[^{223}Ra]$RaCl_2$ uptake in bone was rapid and stable. We observed persistent localization at bone epiphyses, as well as the red pulp of the spleen, while its uptake in most soft tissues cleared within 24 h. [^{223}Ra]$RaCl_2$ distribution in soft tissues is similar in all age groups tested, while bone activity significantly decreased with aging. Although the diagnostic tracers cleared much faster from soft tissues than the therapeutic radionuclide, [^{99m}Tc]Tc-MDP and [^{18}F]NaF both co-localized with [^{223}Ra]$RaCl_2$ in the skeletal compartment.

*Correspondence: co-corresponding authors: Dr. Diane Abou, 733 North Broadway, Traylor 210, Baltimore, MD 21205, dabou1@jhmi.edu. Dr. Daniel Thorek, 720 Rutland Ave. Ross Building 220 Baltimore, MD 21205, dthorek1@jhmi.edu.

Conclusions—Radium-223 localization to the bone is dependent on age-varying factors, which implies that radium-223 dosimetry should take patient age into account. [^{99m}Tc]Tc-MDP shows a different biodistribution from [^{223}Ra]$RaCl_2$, both in soft tissues and in bone. [^{18}F]NaF presents a high similarity with [^{223}Ra]$RaCl_2$ in skeletal uptake, which validates the potential of [^{18}F]NaF as an imaging surrogate to predict radium-223 radiotherapeutic distribution in bone.

Introduction

Prostate cancer is the most common cancer among men in the United States [1]. In most men with castration-resistant prostate cancer – the lethal stage of the disease that no longer responds to hormone therapy – cancer frequently metastasizes to the bone [2]. Bone metastases degrade patient's quality of life, causing severe pain, bone fractures, spinal cord compression, hypercalcemia, decreased stability and impaired mobility [3]. Apart from prostate cancer, bone metastases are common for bone-avid cancers of the breast, lungs, thyroid and kidney [4].

Treatment options for bone metastases have historically been limited mainly to palliative pain control. Among these treatment options, internal radiotherapy using specifically localized bone-seeking radiopharmaceuticals has proven to be an effective method to reduce pain and skeletally related events [5]. Historically approved beta particle emitting radiopharmaceuticals for clinical use are Strontium-89 chloride ([^{89}Sr]Sr-chloride; Emtastron) and Samarium-153 ethylenediaminetetramethylene phosphonic acid ([^{153}Sm]Sm-EDTMP; Lexidronam/Quadramet) [6]. They have different mechanisms as bone seekers: [^{89}Sr]Sr-chloride is a calcimimetic agent, whereas [^{153}Sm]Sm-EDTMP is a phosphonate-based agent. However, these agents have not resulted in increased survival. Recent developments with an experimental beta emitting bone agent ([188Re]Re-HEDP) have shown survival benefit but future work is required before approval by FDA and EMA [7]. Further, given the mean beta particle path length of 0.7 cm for strontium-89 and 0.33 cm for samarium-153, bone marrow toxicity may be a concern when they localize to sites of disease at the bone surface [8].

Recently, radium-223 dichloride was introduced, the first alpha (α)-particle emitting radiopharmaceutical approved by the FDA and EMA for treatment of bone-metastatic, castration-resistant prostate cancer [9]. A phase 3 trial involving 921 patients showed that radium-223, as compared with placebo, significantly prolonged overall survival (median, 14.9 months vs. 11.3 months) [10]. In contrast to beta-emitters, an alpha particle has a much denser and shorter ionization track, resulting in irreversible DNA damage while sparing off-target sites [11].

Radium is a bone-seeker, like other elements in the alkaline earth series of the periodic table (Ca, Sr, and Ba). Ra^{2+} has a very high affinity for hydroxyapatite crystals in the mineral bone matrix, and may selectively localize at sites of increased bone turnover. The approved isotope, radium-223, can be produced from source Actinium-227/Thorium-227 [12, 13]. Radium-223 has a physical half-life of 11.4 days, which enables easy transportation and clinical application. Most importantly, radium-223 emits 96% of energy in the form of alpha

particles. These properties above all have made radium-223 an effective agent to combat bone metastases [10, 14–17].

To date, radium-223 dichloride is administered on a per mass basis, irrespective of patient disease characteristics [18]. A better understanding of the properties of [^{223}Ra]$RaCl_2$ may help shed light on patient-specific prescription and dosimetry. First, we wanted to assess the clearance of the radionuclide from soft-tissues and determine the redistribution occurring in bone. Patients with bone metastatic prostate cancer are predominantly geriatric. Aging brings with it whole-body metabolic changes, which have a direct impact on structural and biochemical bone characteristics that may play a role in specific localization of radium-223. In this study, we investigated [^{223}Ra]$RaCl_2$ pharmacokinetics in mice of increasing age, in which bone features with respect to aging are well described, in order to assess how aging and bone maturity affect its biodistribution.

Another question arising from clinical observations of [^{223}Ra]$RaCl_2$ treatments is how to determine its distribution in patients for theragnostic information. Radium-223 is a high energy alpha particle emitter, but releases only few imageable positrons or gamma rays, compromising its imaging potential. In contrast, [^{99m}Tc]Tc-methylene diphosphonate ([^{99m}Tc]Tc-MDP) and [^{18}F]sodium fluoride ([^{18}F]NaF) are widely clinically utilized imaging agents with tropism to sites of active bone remodeling [19–21]. Combining the gamma rays emitted by technetium-99m and the hydroxyapatite affinity of diphosphonates, [^{99m}Tc]Tc-MDP is applied in bone scintigraphy and single photon emission computed tomography (SPECT). For [^{18}F]NaF, the OH^- ion can be exchanged for [^{18}F]F^- on the surface of the hydroxyapatite matrix of the bone to form fluoroapatite, providing localized positron emission signal for PET. Given the common bone-seeking properties of the three radiopharmaceuticals, we undertook studies to determine the comparability of whole-body and microstructural localization between [^{223}Ra]$RaCl_2$ and [^{99m}Tc]Tc-MDP, or between [^{223}Ra]$RaCl_2$ and [^{18}F]NaF, aiming to define a diagnostic imaging agent surrogate to predict the biodistribution of the therapeutic agent [^{223}Ra]$RaCl_2$.

Methods

Animal Experiments

All mice were male C57Bl/6 mice, aging from 7 weeks old, 15 weeks old, 30 weeks old, to 22 months old; purchased from Harlan Laboratories (Frederick, MD). Mice were placed on standard feed *ad libitum*. All mouse experimentation was performed following institutional animal welfare protocols at The Johns Hopkins University School of Medicine (protocol # MO16M433).

Radiopharmaceuticals were administered to anesthetized mice via retro-orbital sinus (n=5 per experiment group). Mice dosed with [^{223}Ra]$RaCl_2$ 3.7 kBq (100 nCi) were sacrificed at 1 h, 2 h, and 24 h post administration for prompt dissection, where indicated. Mice administered [^{99m}Tc]Tc-MDP 3700 kBq (100 μCi) were sacrificed at 2 h post administration and those with [^{18}F]NaF 370 kBq (10 μCi) were sacrificed at 1 h post administration; for prompt dissection. Whole-body distribution was evaluated from organs including blood, heart, lungs, liver, spleen, kidney, stomach, cecum, small intestines, muscle, epididymal fat,

and tibia (including fibula). Organ radioactivity was assessed by gamma counting (see below). One leg from each mouse was cryo-embedded (OCT, Sakura Fintec, Torrance, CA) without decalcification procedures to prevent bone radiolabel-loss and sectioned (below).

For expanded skeletal dissection and biodistribution, mice (n=5) were euthanized by CO_2 asphyxiation at 24h post-injection of 3.7 kBq (100 nCi) [^{223}Ra]$RaCl_2$, and immediately dissected to collect bones. Skin, organs and soft tissues were trimmed, long bones were separated at the joints and the vertebral column was separated into cervical, thoracic, lumbar, sacral and tail after the pelvic girdle was removed. The ribcage and sternum were removed from the spinal column. The limbs were separated into long bone segments and paw. The mandible was removed from the skull, which was divided into two portions - caudal half including the calvarium and rostral half including maxilla and the nasal cavity.

Biodistribution Gamma Counting

2480 WIZARD^2 automatic gamma counter (Perkin Elmer; Waltham, MA) was used for gamma counting to quantitatively evaluate the radioactivity distribution in each organ. Radiopharmaceuticals with 10% of injected radioactivity were prepared as standard samples for gamma counting. The three isotopes, radium-223, technetium-99m, and fluorine-18, were counted using individual protocols for 60 seconds. Counting windows were 270–300 keV, 121–159 keV, 250–700 keV respectively. Data were normalized to organ weight as percent injected activity per gram (%IA/g).

Statistical analysis

Results are presented as mean ± standard deviation. Statistical evaluation was performed in Excel (Microsoft; Redmond, WA) and Prism 7 (GraphPad Software; La Jolla, CA). For multiple-group-evaluation($n \geq 3$), single factor Analysis of Variance (ANOVA) test was first performed to determine statistical differences among groups. Further, statistical difference between two groups was assessed using unpaired two-tailed Student's t-test. $p<0.05$ is denoted as significant difference, and $p<0.01$ is denoted as highly significant difference.

Histology

The cryo-embedded hind limbs were sectioned with 10 μm thickness on adhesive support [22]. Cryo-embedded spleens were also cut to 10 μm thick sections. Autoradiography was performed on the sections using a Cyclone PhosphorImager (Perkin Elmer; Waltham, MA).

For histochemical development, slides were fixed with formalin for 10 min, followed by a PBS rinse for 5 min. Then the slides were stained with hematoxylin for several seconds, rinsed by PBS for 5 min, and washed with flowing water for more than 10 min. Next, the slides were stained with eosin for 5 seconds, and washed with flowing water for more than 10 min. Stained sections were mounted under coverslip with 30% glycerol.

The alkaline phosphatase staining procedure used a freshly prepared solution of naphtol phosphate (0.05 mg/mL); fast red (1 mg/mL) in Tris buffer (0.08M) pH 9. Sections were fixed in 100% ethanol, rinsed with PBS for 5 min and stained in the solution for 1 h at 37° C. The stained slides were allowed to cool to room temperature for 15 min. Counter staining

with hematoxylin for 15 seconds was followed by a gentle flowing water wash and 1 min PBS rinse. After a final rinse with water samples were mounted under coverslip with 30% glycerol.

Results

Biodistribion of [^{223}Ra]$RaCl_2$ with Time

To explore how [^{223}Ra]$RaCl_2$ distribution in mice varies with time, we first examined the kinetic biodistribution of [^{223}Ra]$RaCl_2$ in skeletally mature mice (C57Bl/6 aged 15 weeks) (Figure 1A). Mice were sacrificed at 1, 2 and 24 h post-injection (p.i.). Radium-223 uptake in bone (fibula and tibia) was rapid and remained unchanged over time. Radium-223 greatly accumulated in these bones as early as 1 h post-injection and no significant difference was found in bone uptake across the window of 1 to 24h ($p=0.96$). The uptake at 24 h across a wider sampling of skeletal components is included as Supplemental Figure 1. This demonstrates distributed bone uptake across sites of active bone remodeling including the spinal column and skull bones. The distribution of radium-223 at 1, 2 and 24 h on a %IA basis, not normalized to tissue mass is presented as Supplemental Figure 2.

Besides the prominent osseous uptake, other organs showed noticeable accumulation of radium-223. These include the spleen, kidney, stomach, cecum and small intestine. In contrast to bone, radium-223 uptake in soft tissues varied with time. For instance, at 1 h p.i., radium-223 uptake in kidneys has non-significant difference from that measured in the bone samples ($p=0.40$ in a student's t-test). However, radium-223 uptake in kidneys dramatically and rapidly decreased, reflecting renal clearance. radium-223 uptake in cecum peaked at 2 h p.i. and greatly decreased at 24h p.i. correlating with bowel excretion. While the radioactivity largely cleared soft tissues within 24 h, radium-223 remained in the spleen.

The microscopic distribution of radium-223a was also assessed. Intact hind limbs of mice were cryosectioned without decalcification, scanned for autoradiography and subsequently stained with hematoxylin and eosin. [^{223}Ra]$RaCl_2$ dosed mice sacrificed at different time points post administration were studied. Representative sections are shown in Figure 1(B): *en* bloc macrographs show the cross sections of embedded samples; H&E staining images show the histological structure of the 10 μm thick leg samples; and autoradiographs acquired of the 10 μm thick sections show the localization of radium-223 within a leg. radium-223 and daughters exclusively localized in mineralized tissues, rather than surrounding muscle, verifying the results from quantitative biodistribution (Figure 1A). A greater accumulation of radium-223 is noted along the bone surface. In particular, the ossifying fronts adjacent the femur and tibia at the knee joint have the highest accumulation of radium-223, while cortical tibia and femur present less activity. These results correlate previously reported research [22].

Splenic localization of [^{223}Ra]$RaCl_2$

Non-negligible uptake of radium-223 was found in soft-tissues, Figure 1A. Specifically, a significant amount of radium-223 accumulated in the spleen at 24 h post administration, while radium-223 in other soft tissues has cleared. To further explore radium-223

microdistribution in the spleen, we microscopically evaluated H&E stained spleen sections and correlated with autoradiography (Figure 2). H&E staining shows white pulp (purple) and red pulp (pink) in the spleen. The majority of activity localized in the red pulp, which is constituted of red blood cells and nucleated cells including macrophages and endothelial cells. The lack of persistent activity in the blood or bone marrow suggests that neither red blood cells nor hematopoietic cells are associated with retained radium-223 in the spleen.

Age Dependent Localization of [^{223}Ra]$RaCl_2$

Based on the kinetic biodistribution of [^{223}Ra]$RaCl_2$ previously shown over 24h, no significant difference in bone uptake or clearance was seen with time. Thus, we chose 2 h post administration as the standard time point to evaluate the effect of age in radium-223 distribution.

With increasing age, radium-223 uptake in bone decreases, from 25.06%IA/g in 7 week old mice, 16.97%IA/g in 15 week old mice, 14.50%IA/g in 30 week old mice, to 12.87%IA/g in 22 month old mice. There is significant decrease from 7 week old to 30 week old, and from 7 week old to 22 month old ($p<0.05$). student's t-tests also show that there is highly significant decrease from 15 week old to 22 month old ($p<0.01$). The distribution on a %IA basis, not normalized to tissue mass is presented as Supplemental Figure 3.

Several other organs show significant uptake of radium-223, including spleen, kidney, stomach, cecum, and small intestine. ANOVA testing showed that among the age groups, radium-223 uptake in these organs have non-significant differences ($p>0.05$), excluding the kidney ($p<0.01$). There is a significant increase kidney uptake in elder mice. Thus, aging results in a significant difference in bone uptake, but not among soft tissues and other organs (except kidneys).

We next explored the microscopic radium-223 distribution in differently aged C57Bl/6 mice. 7 week old mice are representative of juvenile (not skeletally mature) mice. 15 week old and 30 weeks old mice are skeletally mature adult mice and 22 months old animals have decreased bone mass and lowered bone quality [23, 24]. Autoradiography of the intact tibia and femur show that radium-223 exclusively localized in bone, not in surrounding muscle. In the youngest three ages (7, 15 and 30 week old mice) the bone adjacent to the epiphyseal plate at the end of the long bones has the greatest signal. However, no specific localization was noted behind the growth plates at the 22 month old mice.

To further determine the localization of radium-223 within bone, alkaline phosphatase (ALP) staining was performed on leg sections of 7 week old and 22 month old mice. Matching results between ALP staining and autoradiogram are shown in Figure 4. Alkaline phosphatase in the bone is a marker of osteoblast activity within the bone [25].. Evidence of cartilaginous growth plates at the proximal tibia and distal femur in the 7 week old mice are seen (Figure 4A). This is a region of intense mineralization, making it a site of high radium-223 incorporation and localization. In contrast, no growth plate was observed in 22 month old mouse leg (Figure 4B), which correlates with the non-specific distribution of radium-223 within bone.

Biodistribution comparison of [^{99m}Tc]Tc-MDP and [^{223}Ra]RaCl$_2$

Aiming to define an imaging agent surrogate to predict radium-223 distribution was quantitatively compared at the whole organ level and microscopically using autoradiography. [^{99m}Tc]Tc-MDP is a commonly used imaging agent for scintigraphy (referred to as a bone scan) and SPECT, and it is imaged 2 h post injection in patients. To compare technetium-99m and radium-223, we checked the biodistribution at 2 h post injection.

Shown in Figure 5A, technetium-99m and radium-223 have their highest uptake in the bone confirming their bone-seeking properties. 15 week old mice have an average uptake in the bone for radium-223 of 16.97 %IA/g (±1.53%IA/g) and 9.33%IA/g (±1.03%IA/g) for technetium-99m. Radium-223 has significant localization in multiple soft tissues, including spleen, kidney, and the gastrointestinal tract, while technetium-99m has limited uptake in these soft tissues, indicating a higher excretion rate. There are highly significant differences ($p<0.01$) of uptake in blood, spleen, cecum, small intestine, and bone, significant differences ($p<0.05$) of uptake in heart, lungs, liver, kidney, and stomach between the two agents. The distribution on a %IA basis, not normalized to tissue mass is presented as Supplemental Figure 4.

We compared the microscopic distribution of technetium-99m and radium-223 in the bone, representative scans shown in Figure 5B. No significant difference in the radiopharmaceutical localization was observed within the mouse leg: the tibia and femur epiphysis have the highest activity and the cortical bone surface has greater activity accumulated than in bone marrow. These results indicate that [^{99m}Tc]Tc-MDP and [^{223}Ra]RaCl$_2$ have qualitatively similar localization at bone surface, despite the significantly greater %IA/g for radium-223 (Figure 5A).

Biodistribution comparison of [^{18}F]NaF and [^{223}Ra]RaCl$_2$

[^{18}F]NaF is a widely used clinical imaging agent in PET, with a standard imaging time point of 1 h post injection. We studied the biodistribution at 1 h post injection to compare [^{18}F]NaF and [^{223}Ra]RaCl$_2$.

Shown in Figure 6A, fluorine-18 and radium-223 are both bone seekers, and show almost the same uptake in bone (16.18%IA/g (±1.86%IA/g) and 16.71%IA/g (±3.75%IA/g) respectively. Distinct from radium-223, fluorine-18 presents limited distribution in soft tissues. Statistical student’s t-test shows that there is no significant difference in cecum, muscle, fat and bone uptake. However, highly significant differences ($p<0.01$) are noted in blood, heart, liver, spleen, kidney, stomach, and small intestine, with significant differences ($p<0.05$) in lungs. The distribution on a %IA basis, not normalized to tissue mass is presented as Supplemental Figure 5.

We also explored the microscopic distribution of the two radiopharmaceuticals, shown in Figure 6B. Both demonstrate intense labeling localized in the tibia and femur epiphysis. The bone surface was delineated in both autoradiographs, indicating relatively higher radiopharmaceutical localization in the periosteum than in the bone marrow. Given the quantitative biodistribution data and autoradiographs, [^{18}F]NaF has a similar distribution with [^{223}Ra]RaCl$_2$ in the bone.

Discussion

Bone-metastatic castration-resistant prostate cancer severely impacts quality of life throughout the disease course. [^{223}Ra]$RaCl_2$ has been approved as a radiopharmaceutical to extend survival. [^{223}Ra]$RaCl_2$ therapy functions by selectively delivery of radiation doses to the bone with limited toxicity and few side effects. Palliation of painful bone metastasis is also one of the benefits. We posit that through improved understanding of the biodistribution properties of [^{223}Ra]$RaCl_2$, we may guide patient-specific dosimetry and therapy. [^{223}Ra]$RaCl_2$ is currently dosed on a patient-mass basis. Through understanding of patient and lesion specific uptake, it may be possible to elevate administered activity levels to achieve improved disease response without increased toxicity. Conversely, we may be able to reduce administered amounts in some patients while retaining tumoricidal effects. Here, we have focused on understanding [^{223}Ra]$RaCl_2$ re-distribution after injection, variation of uptake with age, and the study of imaging radiopharmaceuticals as surrogates to predict [^{223}Ra]$RaCl_2$ localization *in vivo*.

In skeletally mature mice, [^{223}Ra]$RaCl_2$ accumulation in bone is rapid and stable. Radium-223 is a bone seeker, resulting from its chemical similarity to calcium, which is the principal component of the bone matrix. Bone is constantly undergoing remodeling processes, which includes resorption by osteoclasts and bone formation by osteoblasts [26]. Radium-223 accumulated in the inorganic bone matrix along the bone outline. The bone-seeking property is fundamental for internal radiation therapy. Bone metastases can be accompanied with over-active bone-turnover, which attracts high concentration of radium-223 to the metastatic osseous sites. Though we studied healthy mice here, our previously published work showed that in prostate cancer metastatic mice, osteoblastic and osteolytic lesions both result in radioactivity distribution in adjacent osseous sites, with a similar intensity to the background activity at the epiphyses [22]. In models of prostate cancer metastasis, radioactivity does not localize directly within tumors but instead at the apposite bone surface surrounding the bone lesion and regions of bone activity. Radium-223 localization in bone is stable, resulting in the sequestration of the other alpha decaying daughters in the bone matrix, which verifies clinical observations using low-resolution planar scintigraphy [27].

[^{223}Ra]$RaCl_2$ distribution in soft tissues is similar in all age groups tested, while bone activity significant decreased with aging. Autoradiographs of all mice delineated the bone surface, due to bone remodeling regardless of age. ALP staining visualization of the growth plate correlated with the highest accumulation site of [^{223}Ra]$RaCl_2$ in 7 week old mice. This contrasts with the lack of growth plate in the 22 month old mice (Figure 4). The ossification front at the ends of the long bones do not fuse in rodents, however the rate of growth slows with age [23]. Further experiments on the uptake at bone metastatic sites in aged mice may further help to determine characteristics of radium-223 distribution in mouse models. In the perspective of translating our observations to clinical application, bone turnover and local biological bone activity are relevant to radium-223 accumulation.

Non-negligible uptake in spleen, kidney, and gastrointestinal tract were also observed. Clinical cases have reported such uptake in patients as well, primarily within the

gastrointestinal tract, some leading to adverse effects [28]. In mice, radium-223 uptake in most soft tissues had cleared within 24 hours. However, the spleen had persistent radium-223 at 24 h post injection. The spleen provides an important filtering function for the blood and performs important immunological functions. The organ has an open blood circulation: arterial blood flows in through the white pulp, rich in white blood cells, and then transits into an open area – the red pulp, populated by red blood cells, macrophage and other nucleated cells [29]. Activity was concentrated in the region of red pulp. We speculate that entrapment as a consequence of filtration, a key function of the splenic red pulp, or other nucleated cell types is likely. The persistent localization of radium-223 in the red pulp of spleen has not been reported in man. Phase I pharmacokinetic and biodistribution study of radium-223 dichloride in patients did not show a persistent splenic localization [27]. Further investigation of pre- and clinical samples will investigate the reason for this difference. The general whole-body clearance pattern in patients is similar to that in mouse models. Whole-body patient imaging (1 day after injection) showed focal accumulation in bone metastasis and excretion through gastrointestinal tract.

We also tested two clinically utilized bone imaging agents, [^{99m}Tc]Tc-MDP and [^{18}F]NaF, to evaluate their tendency to co-localize with [^{223}Ra]$RaCl_2$. The three radiopharmaceuticals are all incorporated as components of hydroxyapatite during bone formation process. In this study, we were most interested to compare the distribution of the agents at the times that they are used for clinical evaluation at our center; at 2h post injection for [^{99m}Tc]Tc-MDP scintigraphy and 1h post injection for [^{18}F]NaF PET. [^{99m}Tc]Tc-MDP shows a different biodistribution from [^{223}Ra]$RaCl_2$ at 2h post injection. This discrepancy is due to urinary excretion versus bowel movement. Moreover, the bone uptake is quantitatively not comparable (Figure 5). There was a high degree of concordance in bone uptake between [^{18}F]NaF and that of [^{223}Ra]$RaCl_2$ (Figure 6) and it may be practically possible to use [^{18}F]NaF as imaging surrogate to predict radiotherapeutic uptake. There have been limited clinical investigations into the correlation between fluorine-18 uptake and radium-223 uptake in bone metastases, and results demonstrate significant correlations before radium-223 treatment and in serial response to radium-223 treatment [30].

In this study we used mouse models to quantitatively evaluate and compare the biodistribution of different radiopharmaceuticals at the organ level, which revealed large differences in the soft tissue distribution. [^{99m}Tc]Tc-MDP and [^{18}F]NaF can be cleared quickly in soft tissues which is advantageous in imaging agents, so that the background signal is rapidly diminished. Comparatively, the residence of [^{223}Ra]$RaCl_2$ is much longer, which may lead to unanticipated side effects in soft tissues. It is difficult to predict [^{223}Ra]$RaCl_2$ whole-body distribution using [^{99m}Tc]Tc-MDP or [^{18}F]NaF imaging. Therefore, the calculation of absorbed doses to the soft tissues and background organs may not be feasible in the clinical setting using [^{99m}Tc]Tc-MDP or [^{18}F]NaF at the scanning times currently used. The current study focuses on healthy mouse models, and this underlines the further work required in man to determine the clinical feasibility of applying imaging surrogates for clinical practice in patients. One limitation of these studies is that we have explored the biodistribution of imaging agents at clinically relevant time points (standardized for clinical imaging procedures). Evaluation of non-equilibrium distribution

time points may be warranted of the imaging agents for correlates with [^{223}Ra]$RaCl_2$ whole-body localization in future studies.

Conclusions

Our work demonstrates that radium-223 localization to the bone is dependent on bone parameters that vary with age. Further, our investigation of imaging agent surrogates demonstrates that bone uptake comparisons can be drawn, however determination of soft tissue uptake and attendant off target toxicities is currently not possible. The potential of [^{18}F]NaF as an imaging surrogate to predict the radium-223 distribution in bone is validated. In the perspective of personalized medicine, taking patient age and [^{18}F]NaF imaging performance into account can be beneficial to planning [^{223}Ra]$RaCl_2$ radiotherapy.

Supplementary Material

Refer to Web version on PubMed Central for supplementary material.

Acknowledgments

This work was completed in part through funds from the SNMMI Junior Faculty Award (DSA), Steve Wynn Prostate Cancer Foundation Young Investigator Award (PCF-YIA, DT), the Patrick C. Walsh Fund and the Johns Hopkins University Cancer Center Prostate Cancer SPORE P50CA058236 (DT), and NIH R01CA201035 (DT).

References

1Siegel RL, Miller KD, Jemal A. Cancer Statistics, 2017. CA Cancer J Clin. 2017; 67:7–30. [PubMed: 28055103]

2Sturge J, Caley MP, Waxman J. Bone metastasis in prostate cancer: emerging therapeutic strategies. Nat Rev Clin Oncol. 2011; 8:357–68. [PubMed: 21556025]

3Coleman RE. Metastatic bone disease: clinical features, pathophysiology and treatment strategies. Cancer Treat Rev. 2001; 27:165–76. [PubMed: 11417967]

4Roodman GD. Mechanisms of bone metastasis. Discov Med. 2004; 4:144–8. [PubMed: 20704976]

5Lewington VJ. Bone-seeking radionuclides for therapy. J Nucl Med. 2005; 46(Suppl 1):38S–47S. [PubMed: 15653650]

6Goyal J, Antonarakis ES. Bone-targeting radiopharmaceuticals for the treatment of prostate cancer with bone metastases. Cancer Lett. 2012; 323:135–46. [PubMed: 22521546]

7Biersack HJ, Palmedo H, Andris A, Rogenhofer S, Knapp FF, Guhlke S, et al. Palliation and survival after repeated (188)Re-HEDP therapy of hormone-refractory bone metastases of prostate cancer: a retrospective analysis. J Nucl Med. 2011; 52:1721–6. [PubMed: 21976530]

8Pandit-Taskar N, Larson SM, Carrasquillo JA. Bone-seeking radiopharmaceuticals for treatment of osseous metastases, Part 1: alpha therapy with 223Ra-dichloride. J Nucl Med. 2014; 55:268–74. [PubMed: 24343987]

9Nilsson S. Radionuclide Therapies in Prostate Cancer: Integrating Radium-223 in the Treatment of Patients With Metastatic Castration-Resistant Prostate Cancer. Curr Oncol Rep. 2016; 18:14. [PubMed: 26779616]

10Parker C, Nilsson S, Heinrich D, Helle SI, O'Sullivan JM, Fossa SD, et al. Alpha emitter radium-223 and survival in metastatic prostate cancer. N Engl J Med. 2013; 369:213–23. [PubMed: 23863050]

11Bruland OS, Nilsson S, Fisher DR, Larsen RH. High-linear energy transfer irradiation targeted to skeletal metastases by the alpha-emitter 223Ra: adjuvant or alternative to conventional modalities? Clin Cancer Res. 2006; 12:6250s–7s. [PubMed: 17062709]

12Abou DS, Pickett J, Mattson JE, Thorek DLJ. A Radium-223 microgenerator from cyclotron-produced trace Actinium-227. Appl Radiat Isot. 2017; 119:36–42. [PubMed: 27835737]

13Henriksen G, Hoff P, Alstad J, Larsen RH. 223Ra for endoradiotherapeutic applications prepared from an immobilized 227Ac/227Th source. Radiochimica Acta. 2001:661.

14Henriksen G, Breistol K, Bruland OS, Fodstad O, Larsen RH. Significant antitumor effect from bone-seeking, alpha-particle-emitting (223)Ra demonstrated in an experimental skeletal metastases model. Cancer Res. 2002; 62:3120–5. [PubMed: 12036923]

15Cheetham PJ, Petrylak DP. Alpha particles as radiopharmaceuticals in the treatment of bone metastases: mechanism of action of radium-223 chloride (Alpharadin) and radiation protection. Oncology (Williston Park). 2012; 26:330–7. 41. [PubMed: 22655525]

16Larsen RH, Saxtorph H, Skydsgaard M, Borrebaek J, Jonasdottir TJ, Bruland OS, et al. Radiotoxicity of the alpha-emitting bone-seeker 223Ra injected intravenously into mice: histology, clinical chemistry and hematology. In Vivo. 2006; 20:325–31. [PubMed: 16724665]

17Nilsson S, Larsen RH, Fossa SD, Balteskard L, Borch KW, Westlin JE, et al. First clinical experience with alpha-emitting radium-223 in the treatment of skeletal metastases. Clin Cancer Res. 2005; 11:4451–9. [PubMed: 15958630]

18Du Y, Carrio I, De Vincentis G, Fanti S, Ilhan H, Mommsen C, et al. Practical recommendations for radium-223 treatment of metastatic castration-resistant prostate cancer. Eur J Nucl Med Mol Imaging. 2017; 44:1671–8. [PubMed: 28631036]

19Blake GM, Park-Holohan SJ, Cook GJ, Fogelman I. Quantitative studies of bone with the use of 18F-fluoride and 99mTc-methylene diphosphonate. Semin Nucl Med. 2001; 31:28–49. [PubMed: 11200203]

20Even-Sapir E, Metser U, Mishani E, Lievshitz G, Lerman H, Leibovitch I. The detection of bone metastases in patients with high-risk prostate cancer: 99mTc-MDP Planar bone scintigraphy, single- and multi-field-of-view SPECT, 18F-fluoride PET, and 18F-fluoride PET/CT. J Nucl Med. 2006; 47:287–97. [PubMed: 16455635]

21Jadvar H, Desai B, Conti PS. Sodium 18F-fluoride PET/CT of bone, joint, and other disorders. Semin Nucl Med. 2015; 45:58–65. [PubMed: 25475379]

22Abou DS, Ulmert D, Doucet M, Hobbs RF, Riddle RC, Thorek DL. Whole-Body and Microenvironmental Localization of Radium-223 in Naive and Mouse Models of Prostate Cancer Metastasis. J Natl Cancer Inst. 2016:108.

23Jilka RL. The relevance of mouse models for investigating age-related bone loss in humans. J Gerontol A Biol Sci Med Sci. 2013; 68:1209–17. [PubMed: 23689830]

24Halloran BP, Ferguson VL, Simske SJ, Burghardt A, Venton LL, Majumdar S. Changes in bone structure and mass with advancing age in the male C57BL/6J mouse. J Bone Miner Res. 2002; 17:1044–50. [PubMed: 12054159]

25Miao D, Scutt A. Histochemical localization of alkaline phosphatase activity in decalcified bone and cartilage. J Histochem Cytochem. 2002; 50:333–40. [PubMed: 11850436]

26Raggatt LJ, Partridge NC. Cellular and molecular mechanisms of bone remodeling. J Biol Chem. 2010; 285:25103–8. [PubMed: 20501658]

27Carrasquillo JA, O'Donoghue JA, Pandit-Taskar N, Humm JL, Rathkopf DE, Slovin SF, et al. Phase I pharmacokinetic and biodistribution study with escalating doses of (2)(2)(3)Ra-dichloride in men with castration-resistant metastatic prostate cancer. Eur J Nucl Med Mol Imaging. 2013; 40:1384–93. [PubMed: 23653243]

28Jadvar H, Challa S, Quinn DI, Conti PS. One-Year Postapproval Clinical Experience with Radium-223 Dichloride in Patients with Metastatic Castrate-Resistant Prostate Cancer. Cancer Biother Radiopharm. 2015; 30:195–9. [PubMed: 25746633]

29Cesta MF. Normal structure, function, and histology of the spleen. Toxicol Pathol. 2006; 34:455–65. [PubMed: 17067939]

30Murray I, Chittenden SJ, Denis-Bacelar AM, Hindorf C, Parker CC, Chua S, et al. The potential of (223)Ra and (18)F-fluoride imaging to predict bone lesion response to treatment with (223)Ra-dichloride in castration-resistant prostate cancer. Eur J Nucl Med Mol Imaging. 2017

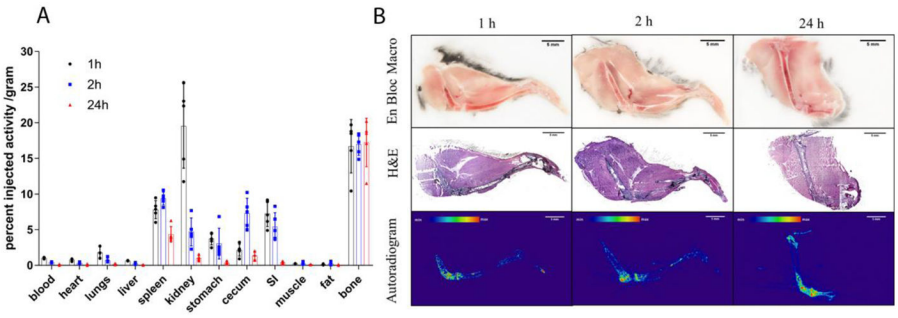

Figure 1.

Acute biodistribution of [^{223}Ra]$RaCl_2$ in healthy C57Bl/6 mice. (A) Replicates (n=5) of gamma counted organs at 1 h (black circle), 2 h (blue square) and 24 h (red triangle) after intravenous administration by the retro-orbital sinus to 15 week old male mice. Data are plotted as counts normalized to the initial injected activity (3.7kBq, 100 nCi) and tissue or blood weights ± standard deviation (SD). (B) Undecalcified whole-mount cryosection and autoradiography of mouse legs: *en* block color macrophotographs of embedded samples at the cutting surface; Hematoxylin & Eosin staining images of 10 μm thick sections; autoradiographs acquired on the 10 μm thick sections. Scale bars=5mm.

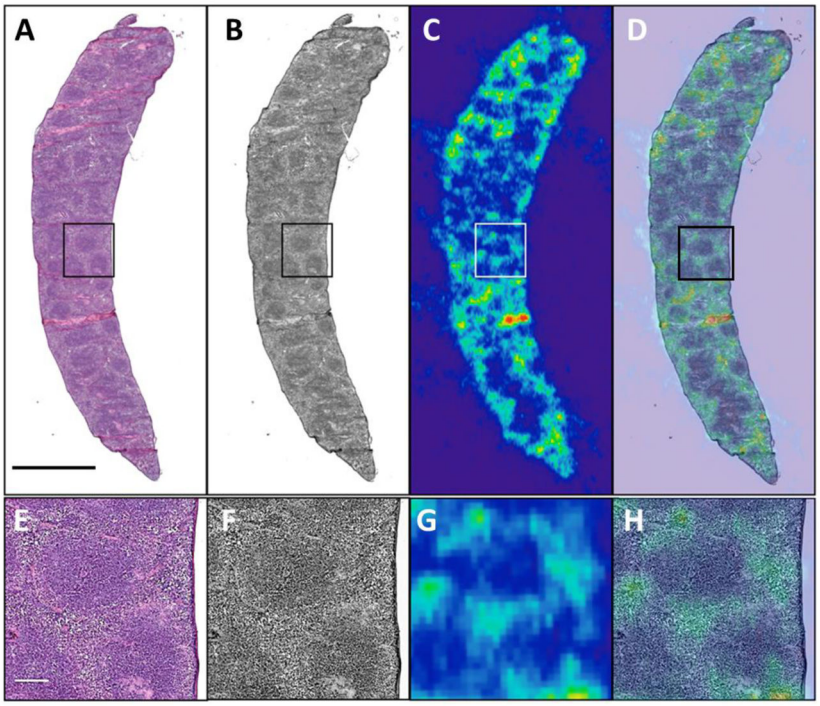

Figure 2.

Spleen of 15 week old healthy C57Bl/6 mouse. Mouse was sacrificed at 2 h after retro-orbital intravenous administration of [^{223}Ra]$RaCl_2$. (A) H&E staining depicts white pulp (purple) and red pulp (pink); (B) greyscale H&E staining image; (C) corresponding autoradiograph of spleen; (D) overlay of H&E and the autoradiograph. Images (A–D) share a scale bar of 2mm. (E–H) magnified inset region of the spleen shown in the box imposed on (AD). Images (E–H) share a scale bar of 200 μm.

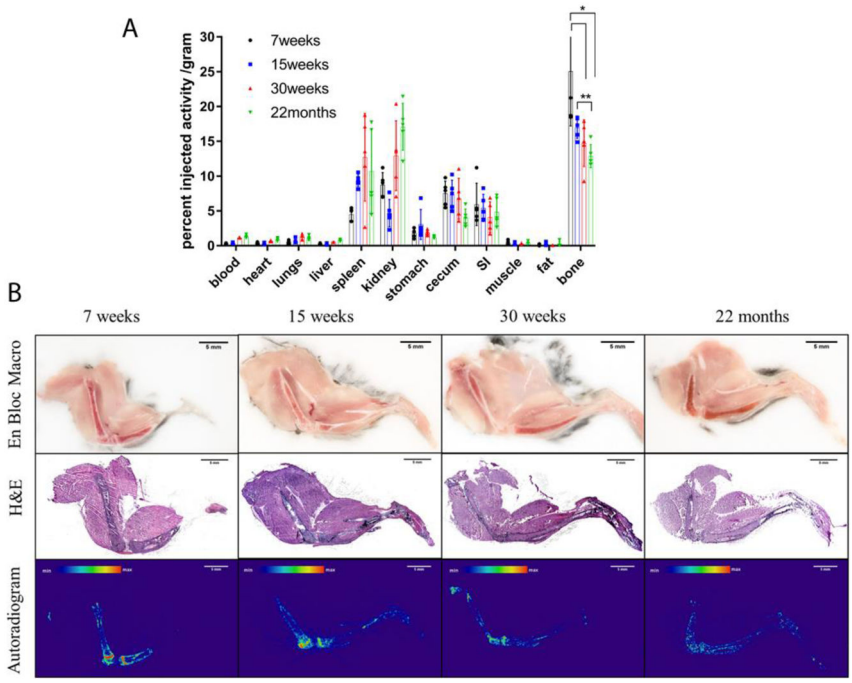

Figure 3.

Biodistribution of [^{223}Ra]$RaCl_2$ in healthy C57Bl/6 mice of different age. (A) Replicates (n=5) of gamma counted organs at 2h after intravenous administration by the retro-orbital sinus to 7 week old (black circle), 15 week old (blue square), 30 week old (red triangle), and 22 month old (green triangle) male mice. Data are plotted as counts normalized to the injection activity (3.7kBq, 100 nCi) and tissue weights ± standard deviation. * denotes significant difference ($p<0.05$). ** denotes highly significant difference ($p<0.01$). Bone = tibia and fibula. (B) Undecalcified whole-mount cryosection and autoradiography of different aged [^{223}Ra]$RaCl_2$ dosed C57Bl/6 mouse legs: *en* block color macrophotographs of embedded samples at the cutting surface; H&E staining images of the 10 μm thick sections; autoradiographs acquired on the 10 μm thick sections. Scale bars=5mm.

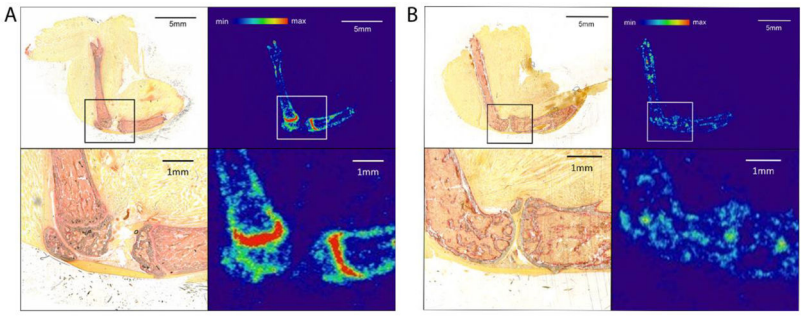

Figure 4.

Comparison of [^{223}Ra]$RaCl_2$ biodistribution in 7 week old and 22 months mice. Both mice were sacrificed at 2 h after retro-orbital intravenous administration of [^{223}Ra]$RaCl_2$. Mouse legs were undecalcified and cryosectioned into 10 μm thick sections. (A) Alkaline phosphatase (ALP) staining and autoradiograph of 7 week old mouse leg section. (B) ALP staining and autoradiograph of 22 months old mouse leg section. Osteoblasts along the surface of cortical and trabecular bone are red in ALP staining.

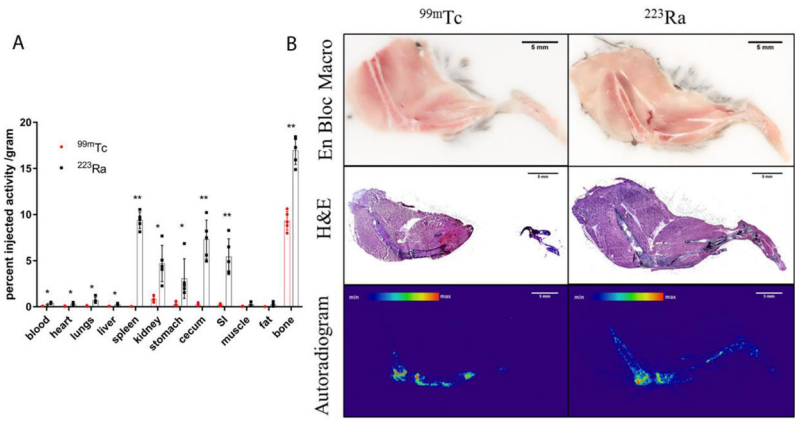

Figure 5.

Comparative biodistribution of [^{99m}Tc]Tc-MDP and [^{223}Ra]$RaCl_2$ in healthy C57Bl/6 mice. (A) Replicates (n=5) of gamma counted organs at 2 h after intravenous administration by the retro-orbital sinus to 15 week old male mice. Data are plotted as counts normalized to the injection activity (3.7 kBq (100 nCi) for radium-223 and 3.7 MBq (100 μCi) for technetium-99m) and mass of tissue or blood excised ± standard deviation. Statistical student's t-test was performed between two agents on each organ. * denotes significant difference ($p<0.05$). ** denotes highly significant difference. Bone = tibia and fibula. (B) Undecalcified whole-mount cryosection and autoradiography of different agent dosed mouse legs: en block color macrophotographs of embedded samples at the cutting surface; H&E staining images of the 10 μm thick sections; autoradiographs acquired on the 10 μm thick sections. Scale bars=5mm.

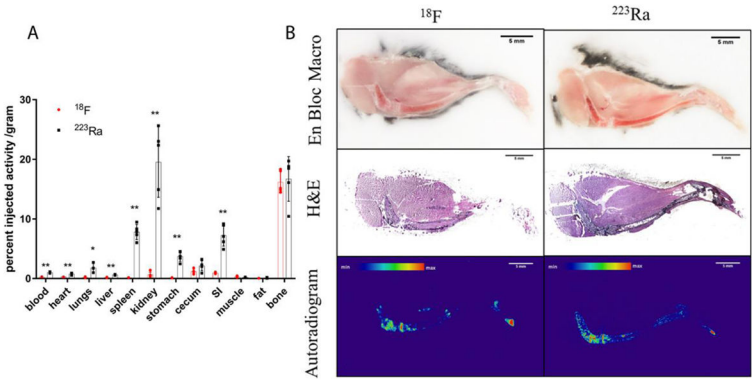

Figure 6.

Biodistribution comparison of [^{18}F]NaF and [^{223}Ra]$RaCl_2$ in healthy C57Bl/6 mice. (A) Replicates (n=5) of gamma counted organs at 1 h after intravenous administration by the retro-orbital sinus to 15 week old male mice. Data are plotted as counts normalized to the injection activity (3.7kBq (100 nCi) for [^{223}Ra]$RaCl_2$ and 370 kBq (10 μCi) for [^{18}F]NaF) and mass of tissue or blood excised ± standard deviation. Statistical student's t-test was performed between two agents on each organ. * denotes significant difference ($p<0.05$). ** denotes highly significant difference. Bone = tibia and fibula. (B) Undecalcified whole-mount cryosection and autoradiography of different agent dosed mouse legs: en block color macrophotographs of embedded samples at the cutting surface; H&E staining images of the 10 μm thick sections; autoradiographs acquired on the 10 μm thick sections. Scale bars=5mm.